Computers and Electronics in Agriculture 224 (2024) 109128

Contents lists available at ScienceDirect

Computers and Electronics in Agriculture

journal homepage: www.elsevier.com/locate/compag

Original papers

Remotely sensing inner fruit quality using multispectral LiDAR: Estimating sugar and dry matter content in apples

Tomislav Medic [a,*], Pabitro Ray [a], Yu Han [a], Giovanni Antonio Lodovico Broggini [b], Simon Kollaart [c]

[a] Institute of Geodesy and Photogrammetry, ETH Zurich, Stefano-Franscini-Platz 5, 8093 Zurich, Switzerland
[b] Molecular Plant Breeding, Institute of Agricultural Sciences, ETH Zurich, Universitaetstrasse 2, 8092 Zurich, Switzerland
[c] Agroscope, Müller-Thurgau-Strasse 29, 8820 Wädenswil, Switzerland

ARTICLE INFO

Keywords:
Point clouds
Chemometrics
Spectroscopy
Reflectance
Soluble solid content
Hyperspectral

ABSTRACT

Diffuse reflectance spectroscopy is a well-established non-destructive technique for in-situ estimation of internal fruit quality properties. However, the operating range of the conventionally used instruments is limited to a few cm and often requires direct surface contact with the fruit. Alternative non-destructive approaches, such as hyperspectral imaging, allow for space between the sensor and the object, but in return, they require controlled illumination conditions commonly realized using dark chambers. In this work, we present a novel approach toward remote sensing of relevant fruit quality parameters on the case study of estimating total soluble solids (TSS) and dry matter content (DMC) in apples using a prototype supercontinuum-based multispectral LiDAR (MSL). Experimental results are acquired over a stand-off range of 0.5 m under uncontrolled illumination conditions. The spectral data is acquired across the 580–900 nm spectral range of the supercontinuum source, and R^2 of 0.73 is achieved for estimating TSS and DMC using a random forest regression. These results on the estimated parameters are comparable to those reported previously in the literature for in-house developed prototypes relying on fruit contact or immediate proximity. In contrast, our experiments demonstrated TSS and DMC estimation at larger distances relative to typical reflectance spectroscopy instruments and without controlled illumination conditions typically mandated by hyperspectral imaging. Moreover, we demonstrate how our results translate to the estimation of TSS and DMC from experimentally generated multispectral 3D point clouds at a stand-off range of 5 m, demonstrating the potential of simultaneous acquisition of spectral and geometrical data at even higher ranges, showcasing the possibility of new use-cases.

1. Introduction

Scanning LiDAR (Light Detection and Ranging) is widely used for plant-focused remote-sensing e.g. in agriculture, and forestry (Eitel et al., 2016a; Jin et al., 2021). Traditionally, LiDAR is primarily used to extract structural plant traits by analyzing the geometrical data of 3D point clouds. Despite notable development over the recent years, the reflectance profiles or intensity of backscattered light are still under-exploited (Eitel et al., 2016a), where plant phenotyping could particularly benefit from further advancements (Jin et al., 2021).

Scientific efforts on LiDAR-based spectral plant phenotyping have primarily focused on observing leaf properties, where LiDAR intensity has been successfully used as a proxy for monitoring: leaf water status (Elsherif et al., 2018; Gaulton et al., 2013; Junttila et al., 2021); plant's nutrition status, primarily related to nitrogen concentration (Du et al., 2016; Eitel et al., 2016b); and the status of photosynthetic apparatus (Eitel et al., 2010) together with related chlorophyll fluorescence (Magney et al., 2014). The abovementioned studies used one to two commercial, single-wavelength TLSs (terrestrial laser scanners), while the studies using in-house built multispectral prototypes are emerging (Hakala et al., 2012; Junttila et al., 2015; Sun et al., 2017). In several investigations, multispectral LiDAR (MSL) has been successfully used to extract plant vegetation indices with an accuracy comparable to existing multi- and hyperspectral camera-based techniques (Chen et al., 2010; Hakala et al., 2015; Li et al., 2014; Nevalainen et al., 2014; Niu et al., 2015; Puttonen et al., 2010; Sun et al., 2017). However, MSL offers additional benefits, such as illumination invariance and high measurement ranges, and is thus advantageous for diurnal and in-field observations (Jin et al., 2021), as well as some other niche applications.

* Corresponding author.
E-mail addresses: tomislav.medic@geod.baug.ethz.ch (T. Medic), pabitro.ray@geod.baug.ethz.ch (P. Ray), yu.han@geod.baug.ethz.ch (Y. Han), giovanni.broggini@usys.ethz.ch (G.A.L. Broggini), simon.kollaart@agroscope.admin.ch (S. Kollaart).

https://doi.org/10.1016/j.compag.2024.109128
Received 22 April 2023; Received in revised form 15 February 2024; Accepted 1 June 2024
Available online 10 June 2024

So far only one study investigated the potential of estimating fruit quality using LiDAR intensities (Saha and Zude-Sasse, 2022), where banana ripeness was estimated based on the intensity data obtained with a commercial monochromatic (670 nm) automotive scanner.

Monitoring fruit quality metrics is relevant for different stages of the food production chain, such as plant breeding, tracking fruit health and progress during a growth season, indicating the right harvest time, fruit sorting based on quality parameters related to consumer experience, and monitoring during storage. Some of the relevant quality metrics are related to sugar content or TSS (total soluble solids); titratable acidity, starch content, fruit firmness and texture, internal or external color, and dry matter content (DMC). For example, DMC is an important indicator of fruit maturity and can be used for detecting optimal harvest time (Musacchi and Serra, 2018; Watada, 1993).

Fruit quality parameters are commonly estimated by destructive methods either in the laboratory or during the sorting process using automated machines such as Pimprenelle (Azodanlou, 2001). However, a substantial number of parameters can be estimated using non-destructive techniques as well (Abasi et al., 2018). Some of the most prominent non-destructive methods are imaging methods such as Raman imaging, hyperspectral imaging, magnetic resonance imaging (MRI), and laser light backscattering imaging (LLBI) (Mahanti et al., 2022; Pathmanaban et al., 2019). Although these methods show promising results in controlled laboratory conditions, they are often conducted in dark chambers to mitigate effects due to ambient light variations, exhibit a relatively low throughput, limited or no portability, and have challenges for practical on-tree (on-site) use. Even hyperspectral imaging, routinely used for remote sensing in natural environments (Pu, 2017), suffers from some of these drawbacks when fruit quality estimation is in question (Abasi et al., 2018; Srivastava and Sadistap, 2018). For example, even the state-of-the-art portable solutions, supported by deep learning data processing pipelines, require specialized dark chambers and a relatively short distance to the object (Mishra et al., 2023), limiting the potential use-cases.

In contrast to imaging methods, diffuse reflectance spectroscopy established itself as the most widely used non-destructive method for in-situ observations, including on-tree estimation under the uncontrolled ambient illumination (Abasi et al., 2018; Srivastava and Sadistap, 2018). The method reached high maturity, signalized by the availability of different commercial systems, mostly handheld devices using a broadband light source in the visible (VIS) and near-infrared (NIR) spectrum coupled to a spectrometer (Goisser et al., 2021). Such devices are routinely used for estimating fruit quality parameters, e.g., TSS and DMC of different fruits and vegetables (Goisser et al., 2021). Although offering non-destructive on-site estimation, they require direct contact or high proximity (centimeters) with a fruit, which limits their on-field applicability only to the physically accessible subsets of fruits. Moreover, the data acquisition is relatively time-consuming, limiting the acquired sample size.

MSL presents an alternative approach for non-destructive estimation of fruit quality parameters, addressing the challenges of both hyperspectral imaging and diffuse reflectance spectroscopy. Due to its active sensing principle using the energy-dense and focused laser light of known spectral power profile, it can be deployed in uncontrolled and varying ambient light conditions and can provide point-wise spectral data on larger distances (Vosselman and Maas, 2010). Hence, it enables *remote* reflectance spectroscopy (Hakala et al., 2012) with no fundamental limitations for in-situ and on-tree estimation (Malkamäki et al., 2019). Moreover, if used with a scanning unit on a mobile mapping platform, it allows for on-field remote estimation of fruit quality with high sampling frequency augmented with geometrical data. Such geometrical data can then be used for estimation of further quality parameters, e.g. shape and size, and for directly 3D mapping the distribution of the values of interest and uncovering eventual heterogeneities within a fruit, tree, or orchard. This makes MSL a single-sensor system with relevant capabilities beyond the ones offered by hyperspectral imaging and typical reflectance spectroscopy systems. Employing this technology for in-situ remote estimation of fruit quality would present a relevant contribution toward high-throughput plant phenotyping (HTPP).

Table 1
Summary of the fruit samples information: number of fruits ($F\#$), acquired spectral profiles ($S\#$), mean and standard deviation of total soluble solids (TSS) and dry matter content (DMC) values per cultivar and overall.

Cultivar	$F\#$	$S\#$	$\bar{x}_{TSS}$	$\sigma_{x_{TSS}}$	$\bar{x}_{DMC}$	$\sigma_{x_{DMC}}$
Golden	10	60	12.93	1.35	15.05	1.47
Gala	6	36	11.94	0.95	13.83	1.17
Jazz	5	30	13.39	0.85	15.26	0.90
GD[a]	39	234	16.24	2.91	18.56	3.24
Green Star	10	60	12.93	1.35	13.21	0.58
Pink Lady	9	54	14.44	1.18	16.74	1.07
Juliet	5	30	13.74	1.54	16.20	1.74
Gravenstein	1	6	12.70	0.26	14.70	0.16
ALL	80	480	14.62	2.79	16.83	3.03

[a] GD = Golden Delicious.

Motivated by the latter, we conducted an early investigation of using an MSL, an in-house developed prototype of a mode-locked femtosecond supercontinuum (SC) LiDAR system (Han et al., 2022b; Salido-Monzú and Wieser, 2018), to estimate fruit quality. In particular, we remotely estimate the sugar (TSS) and dry matter content (DMC) of store-bought apples at a stand-off distance of 0.5 m using point-wise LiDAR measurements under uncontrolled ambient light conditions. We analyzed the accuracy of estimating TSS and DMC in the single cultivar and multiple (eight) cultivar cases to test for generalizability and compared the results with the state-of-the-art success of competing instruments. Finally, we paired the prototype with a scanning unit to demonstrate the potential of deriving TSS and DMC from multispectral 3D point clouds of apples at a 5 m stand-off distance.

Hence, to the best of the authors' knowledge, we present the first successful demonstration of using MSL for remote spectroscopy of fruit quality metrics, enabling their estimation under uncontrolled illumination conditions and up to 5 m distances. These results give the first evidence that MSL could be a viable alternative technology for fruit quality estimation, mitigating some of the challenges related to hyperspectral imaging and diffuse reflectance spectroscopy, while simultaneously augmenting these estimates with 3D geometrical data of the analyzed fruits.

This article is structured as follows: Section 2 presents the experimental design 2.1, LiDAR prototype 2.2, acquired data 2.3, and data processing workflow 2.4. Section 3 presents the results of TSS and DMC estimation and demonstration of multispectral scanning. Discussion and main conclusions are presented in Sections 4 and 5.

2. Materials and methods

2.1. Experiment design

Within the experiment, we sampled 80 apples of 8 different cultivars (Table 1) bought in a local supermarket. We acquired spectral profiles using a MSL and reference values for TSS and DMC using the established destructive methods. We followed the experimental design commonly used for calibrating commercial VIS-NIR handheld diffuse reflectance spectrometers for estimating fruit quality metrics, e.g. Zhang et al. (2019). Different cultivars were used to test for the robustness of the estimation method concerning variation within this fruit species. One cultivar had a disproportionally larger number of samples (39 apples, roughly 50%) to test if the estimation accuracy is altered when the regression model is fitted to a particular cultivar, reducing the variability of fruits' properties. The exact number of fruits per cultivar was not pre-determined before the experiment (Section 2.3).

We used a limited number of samples compared to the typical ML (machine learning) regression sample sizes due to limited lab

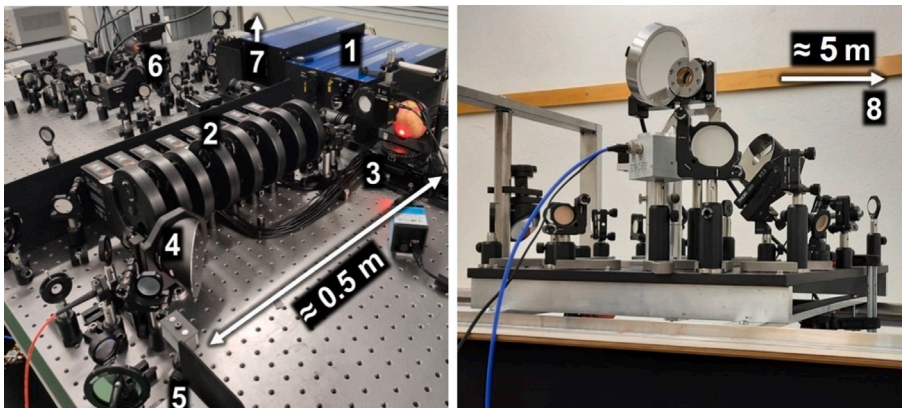

Fig. 1. Left: Experimental setup (1 – laser, 2 – filter wheels, 3 – rotation stage with samples, 4 – parabolic mirror, 5 – APDs, 6 - alternative setup for scanning demo, 7 – indication of the position of scanning unit, 8 – indication of position of scanning samples). Right: Scanning unit.

availability and long measurement duration. Namely, acquiring each spectral profile with a LiDAR prototype took approximately 3 min (Section 2.2). As the spectral measurements are sensitive to temperature (Peirs et al., 2019), the apples were acclimatized in the laboratory under a controlled temperature of 20 °C for around 4 h before the measurements.

A picture of the main laboratory setup is presented in Fig. 1, left. The point-wise spectral measurements for generating the TSS and DMC estimation (regression) model were acquired using the parts of the setup marked with the numbers 1–5, while the remaining part was used later for multispectral scanning (Section 2.2).

The apples were measured at a distance of approximately 0.5 meters (Fig. 1, left) at 3 evenly distributed locations per fruit (to account for the inhomogeneity of the sugar distribution) marked (simple dash) roughly at their equator and separated by approx. 120°. Each location was measured twice with LiDAR: once approx. perpendicular (0°) and once with 20° angle of incidence (AOI) with respect to the line of sight. The angle was altered using a rotation stage (Fig. 1, "3").

Besides collecting redundant observations at each location, this procedure was used for two additional reasons. First, to investigate the sensitivity of the results considering the small changes of incidence angle, as it was indicated as an important influencing factor in the Kaasalainen et al. (2016) and Kaasalainen et al. (2018). Second, the literature indicated possible bias or distortion of the spectral profiles at incidence angles close to 0° due to specular reflection in some cases (Zhu et al., 2015). Implementing this measurement procedure resulted in gathering 6 spectral profiles per fruit (2 × 3 locations) over approx. 20 minutes.

Destructive reference measurements immediately followed spectral data acquisition. We carved out cylindrical samples (2.7 cm in diameter and 2 cm in height) with a borer around the marking indicating the location of spectral measurements as done e.g., in Zhang et al. (2019). This sample diameter is an order of magnitude larger than the laser beam footprint diameter (approximately. 6–8 mm) and the sample height is higher than the nominal penetration depth of the light. However, we presume no rapid changes in TSS and DMC within the fruit, and these sample sizes assured sufficient substance to acquire the measurements with the available instrumentation.

Each apple sample was first peeled and then split into two approximately equal halves. The first half was used for estimating TSS using a digital handheld pocket refractometer for the measurement of soluble solids in fluids (model PAL-1, ATAGO Co., Ltd., Japan). We pressed the apple juice using an ordinary metal kitchen garlic press and applied it to the refractometer. The measurements were repeated three times and averaged (median) to control for eventual errors. The acquired reference values for TSS are expressed in Brix degrees (1 °Brix = 1 g of soluble solids in 100 g of solution), where the instrument's measurement range is from 0 to 60 °Brix, accuracy is ±0.2 °Brix, and resolution 0.1 °Brix. Additionally, the instrument has internal temperature calibration for the readings.

The DMC was calculated as the ratio (%) of the dry and wet mass of the second halves of the cylindrical fruit samples. The samples were weighted using an analytical balance (model KUBEI 996, HuaZhou DaMing Weighing Co., Ltd., China), with a readout resolution of 0.001 g and an accuracy of 0.003 g. The wet weight measurements were done immediately after carving out the sample (preceding the refractometer measurements). The samples were then dried at 65 °C in a fruit dehydrator (Graef model DA506EU) for 24 h and their dry mass was measured as in Kumar et al. (2015).

2.2. Multispectral LiDAR prototype

We present a brief description of the in-house developed MSL (Fig. 1, left), while more detailed information can be found in Han et al. (2022b) and Salido-Monzú and Wieser (2018). A supercontinuum frequency comb laser enclosed in the blue box (Fig. 1, "1") emits coherent light in the range between 580 nm and 900 nm. This spectral range is comparable to the common handheld spectrometers (Goisser et al., 2021) and is thus desirable for sensing fruit quality. Overall 33 *10 nm wide* spectral bands are sequentially transmitted using a set of optical bandpass filters mounted in the rotational filter wheels (Fig. 1, "2"). For each spectral band, 10% of the output power is used to establish a local reference path for distance measurements while the rest 90% is used for probing the fruit samples.

The probing beam interacts with the sampled object (Fig. 1, "3") and the backscattered light is collected and focused on the probing avalanche photodiode - APD (Fig. 1, "5") using a parabolic mirror (Fig. 1, "4"), while the reference beam is directly detected by the reference APD. The distance of the sampled object is estimated by the phase difference between the electric outputs of the two APDs according to the inter-mode beating approach of frequency comb (Minoshima and Matsumoto, 2000; Salido-Monzú and Wieser, 2018). A Spectralon (SG 3070, SphereOptics) reflection standard plate with 60% reflectance flips in and out in front of the sampled object, and the optical intensity backscattered from the plate provides a reference to calculate the reflectance and compensates the time-dependent power variation of the laser source.

The resulting reflectance spectra (Fig. 3, top) were used as the input for the estimation of TSS and DMC and for generating the results presented in Sections 3.1 and 3.2. To ensure the same surface position is probed under the different angles of incidence, the sampled object is mounted on a rotation stage and the sampled position is at the rotation axis (Fig. 1, "3").

The unique feature of the described measurement setup is the possibility to generate spectrally resolved range measurements (Han

et al., 2022b; Salido-Monzú and Wieser, 2018). We investigated if supplementing the reflectance spectra with such range spectra could enhance the TSS and DMC estimation accuracy and the results are presented in Section 3.3.

We also demonstrate that remote estimation of TSS and DMC over several meters is feasible using the proposed supercontinuum laser-based approach. Further experiments are carried out using an in-house developed scanning unit (Fig. 1, right), which is directly coupled to the SC output. The scanning unit allows for spatial mapping of the acquired range and spectral profiles of the target (fruit samples), which is in our case placed 5 m away. Similar to the configuration above, the distance information is estimated by monitoring the relative phase delay of the intermode beats. However, in this case, the target back-reflection is acquired over the entire 580–900 nm band with 0.17 nm spectral resolution using a Czerny-Turner CCD spectrometer (Thorlabs CCS 175). This setup de facto enables hyperspectral laser scanning, however at the expense of losing the abovementioned spectrally resolved range measurements. A detailed description of the scanning unit can be found in Ray et al. (2023). For simplicity, we will refer to the acquired 3D point clouds as multispectral. The initial results that demonstrate the possibility of point-wise (pixel-wise) estimation of TSS and DMC from the acquired 3D point cloud are presented in Section 3.4.

2.3. Acquired data

The reference values for the TSS and DMC are generated as described in Section 2.1, where some observations (less than 1%) were marked as outliers based on the laboratory log and removed from further processing. To acquire an adequate dataset for the regression problem, we aimed at obtaining uniformly distributed TSS and DMC values, avoiding long underrepresented tails at extreme values. This was achieved by real-time adjusting of the sample sizes for different apple cultivars, where the cultivar with the highest variability in the reference values was strongly overrepresented for single-cultivar TSS and DMC predictions. The achieved distributions of the reference values are presented in Fig. 2.

Initial data analysis revealed that the collected reference values for TSS and DMC were highly correlated ($\rho = 98\%$), which is a common occurrence recorded in the literature, e.g. Mcglone et al. (2003). However, TSS and DMC are still used as separate parameters of fruit quality. Hence, there is a high likelihood that the TSS and DMC values we estimated using MSL infer a single joint property of the investigated apple samples. Nevertheless, in the following sections, we present the results for both TSS and DMC for comparability with related literature.

The obtained spectral profiles used to remotely estimate TSS and DMC are presented in Fig. 3. As stated in Section 2.2, we acquired spectrally resolved reflectance and range data, where ranges are normalized by subtracting the mean (absolute values not purposeful due to different apple sizes, and hence the absolute distance to the instrument). The red and blue curves represent medians of 10 uniformly sampled spectral profiles, separated according to TSS (DMC directly comparable) with a spacing of 0.1 °Brix between them, centered around extremely low and extremely high °Brix values (11 °Brix and 19 °Brix). The transparent colors represent the distribution of values as 1x MAD (median absolute deviation from the median).

When analyzing the reflectance spectra, a few clear distinctive features exist between fruits with high and low TSS. One is that the backscattered light has lower intensity across all spectral channels if TSS is low. This is due to less solid and higher water content, as water absorbs light in varying degrees across all observed wavelengths (Vosselman and Maas, 2010). However, using this information requires exhaustive radiometric calibration, i.e., accounting for all external and internal systematic factors causing the fluctuations in the backscattered intensity.

The most prominent spectral feature is a significant reduction in reflectance centered around 670 nm wavelength for low TSS. This

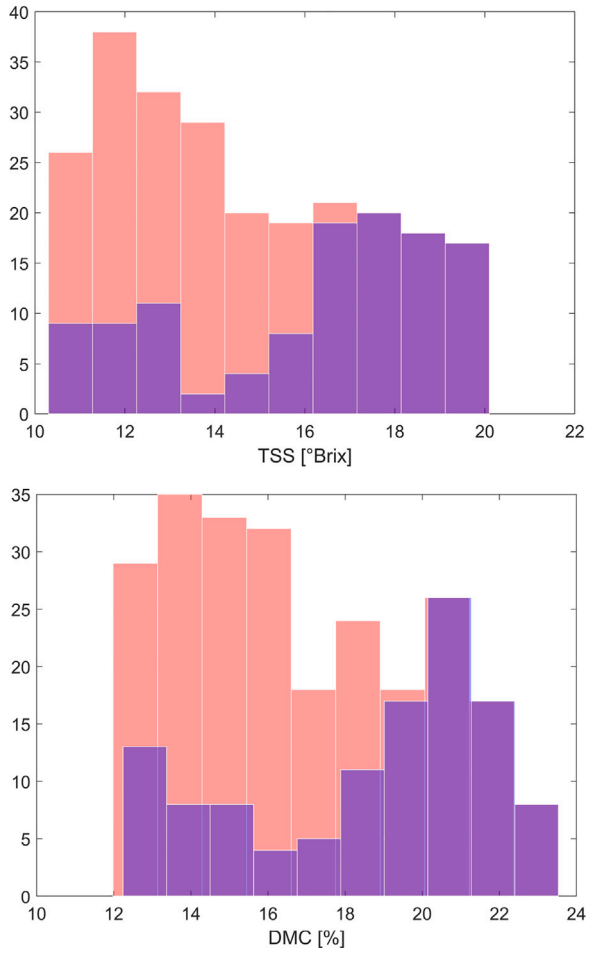

Fig. 2. Histograms of TSS and DMC values; samples of all cultivars together (red) and of overrepresented cultivar alone (purple).

phenomenon can be attributed to a high chlorophyll A concentration in the mesocarp, typically a few mm under the fruit skin. Namely, it is known that chlorophyll A has an absorption peak at 670 nm and its concentrations are highly correlated with some of the relevant fruit properties related to fruit ripening and maturity (Musacchi and Serra, 2018). For example, the study mentioned in the introduction, which focuses on estimating banana ripeness using commercial LiDAR relies on this feature (Saha and Zude-Sasse, 2022). Moreover, IAD, the index of absorption difference between 670 nm and 720 nm, is frequently used for tracking fruit maturity (Musacchi and Serra, 2018). It is commonly done by specialized bichromatic handheld spectrometers (Musacchi and Serra, 2018), e.g. DA Meter (Sinteleia, Bologna, Italy). Hence, we presume that our TSS and DMC estimates will primarily exploit this spectral feature. To confirm and expand these visual observations we conducted a feature importance analysis in Section 3.2.

The range spectra are somewhat less discriminative between low and high TSS fruits. However, the main spectral feature is again the difference at 670 nm, but with higher variability within the TSS classes. This similarity between reflectance and range spectra probably indicates that a drop in power induces a negative systematic shift in range measurements, which could be due to power-to-phase coupling. To analyze this hypothesis we computed the per-wavelength correlations between reflectance and range spectra over all fruit samples. For the wavelengths in the 580–690 nm range, the spectral channels were significantly correlated ($P < 0.01$) with an average correlation of 57%, which indicates that both modalities carry similar information. Because

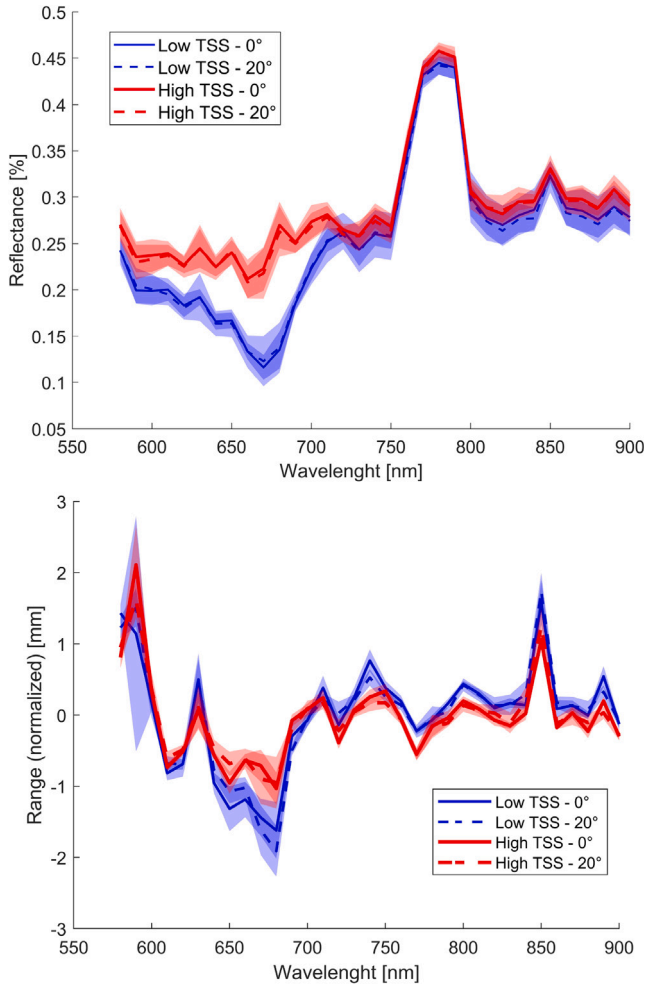

Fig. 3. Apples' reflectance and normalized range spectral profiles: bold lines - median of 10 uniformly sampled profiles centered around extreme TSS values (red – high TSS, blue – low TSS, solid - observations at 0° incidence angle, dashed at 20°); transparent regions – 1x MAD around respective medians.

of that, in Section 3.1, we will primarily focus on the reflectance spectra, which is more generalizable across hyperspectral LiDAR prototypes presented in the literature.

Finally, as visible in Fig. 3, we observed no notable difference between the spectral profiles at 0° and 20° AOIs, alleviating the concerns related to specular reflection (details in Section 2.1). To confirm the visual inspection we computed the correlations (Pearson's) between corresponding spectral profiles at 0° and 20° AOI, which showed an average correlation of 99.3% ($P < 0.01$).

2.4. Data processing

No extensive data transformation and preprocessing were performed on the acquired spectral profiles. Finding the optimal combination of different preprocessing steps, e.g. signal transformations and smoothings, is a part of the ongoing research efforts (Mishra et al., 2021a; Mishra, 2022) and it is out of the scope of our work. However, we made a preprocessing analysis of a limited scope (more at the end of this section).

In our main analysis, we tested 10 different regression approaches for predicting TSS and DMC (Table 2). We tested the possibility of TSS/DMC estimation using a single wavelength, 670 nm (Section 2.3), to check if using a monochromatic LiDAR would be sufficient. Also, we derived the IAD index and used it as a single predicting variable to mimic the handheld IAD meters. Finally, we tested 8 different regression approaches using the full spectrum.

The related works predominantly use PLS (Partial Least Squares), a standard in chemometrics (Wold et al., 2001). Besides PLS, we implemented Lasso linear regression (L1-norm regularization on the coefficients of linear regression), Random Forest (RF), and boosted decision trees algorithm (BOOST) to utilize their inherent capabilities for feature selection (Section 3.2). Feature importance analysis was carried out to better understand the relationship between MSL spectral profiles and variables of interest.

RF and boosted trees were additionally included as they were proven to be the best-performing algorithms for the regression and classification tasks based on simple tabular data with a limited number of explanatory variables (Grinsztajn et al., 2022). Finally, SVM, FFNNs and GPR (Table 2) were added because they can learn more complex functional relationships between variables, and they are better at interpolation than decision trees algorithms.

For the training and evaluation of all regression methods, we used a 20/80% test-train split, where the splits were done on the per-fruit-basis to avoid eventual overfitting if the samples of the same fruit would be present in both test and train datasets. Additionally, for some of the ML approaches (Table 2) we used z-score feature normalization, as it is a recommended procedure for assuring efficient algorithm convergence (LeCun et al., 2012).

We compared the predictive performance of all the algorithms using the common evaluation criteria R^2 value and mean absolute error (MAE). To generate robust estimates and to account for the limited sample size (especially in the case of test data), we repeated the procedure 100 times and reported averaged values for the abovementioned statistical quantities. A subset of the used algorithms allows for hyperparameter tuning. The optimal hyperparameters (Table 2) were searched for using the Bayes optimization algorithm (Snoek et al., 2012) over 200 iterations. A 10-fold cross-validation was implemented to ensure a robust hyperparameter selection while preventing overfitting. The analysis was implemented in MatLab.

We did some preliminary tests on data utilization before the main analysis described above. In these tests (10 instead of 100 runs of the described procedure) we confirmed that using spectral profiles at incidence angles of 0° and 20° as separate explanatory variables does not benefit the estimation. Hence, we pooled all acquired spectral profiles to increase the number of samples for training and testing. Similarly, we verified that applying basic data preprocessing did not noticeably impact the estimation success (abovementioned statistical quantities). More specifically, we tested independently (disregarding eventual interference) following preprocessing procedures that are common in the related literature (Jiao et al., 2020): spectral profiles normalization by subtracting the mean reflectance, generating 1st and 2nd derivative of the spectral profiles, and smoothing the spectrum (moving average, Savitzky–Golay, and Gaussian filters). As a result, no spectral profile preprocessing was applied to obtain the results presented in the following chapter.

3. Results

In Section 3.1 we present the main results of estimating TSS and DMC using reflectance spectra presented in Fig. 3 (top), while Section 3.2 gives related feature importance analysis to better understand the estimation procedure and the observed quantities. In Section 3.3 we analyze if range spectra (see Section 2.2) can support TSS and DMC estimation, while Section 3.4 gives a demonstration of the transferability of our results on multispectral scanning of apples at larger distances.

3.1. Estimating TSS and DMC

The summary of our main findings is presented in Table 3. The analysis from Section 2.4 was done once for all 8 cultivars together

Table 2
Tested regression methods for estimating TSS and DMC: their abbreviations, fixed and tunable (hyper-)parameters (italic = fixed) and an indication of used z-score normalization (Y = Yes, N = No).

#	ABR.	Algorithm	Parameters (tunable, FIXED)	NR.
1	x670	Simple linear regression	*x = 670* nm	N
2	IAD	Simple linear regression	*x = 670/720* nm	N
3	PLS	Partial least squares	*number of components = 20*	N
4	LASSO	Lasso linear regression	Regularization parameter lambda	N
5	RF	Random forest	nr. of learning cycles, min. leaf size, max. number of splits, nr. of variables to sample	N
6	BOOST	Boosted trees	nr. of learning cycles, min. leaf size, max. number of splits, nr. of variables to sample, learn rate	N
7	GPR	Gaussian process regression	basis function, kernel function, kernel scale, sigma	Y
8	SVM	Support vector machines	box constraint, kernel scale, epsilon, *kernel function = gaussian*	Y
9	FFNN	Feed forward neural network	Regularization parameter lambda, layer sizes, layer nr. (1–3), *activation function = sigmoid, fully connected*	Y
10	Esb.	Average solution (#3–9)	–	–

Table 3
Summary of the main results of estimating TSS [° Brix] and DMC [%] with 10 different regression methods (average of 100 runs): generalized regression across 8 apple cultivars ("All Cult."); regression fitted to single cultivar ("Single Cult."); S – single spectra estimates; F – per-fruit mean estimates.

S/F	STATS.	VAR.	X670	IAD	PLS	LASSO	RF	BOOST	GPR	SVM	FFNN	ESB.
All Cult.												
S	R2	TSS	0.24	0.3	0.41	0.48	0.61	0.59	0.58	0.56	0.6	0.64
	R2	DMC	0.25	0.29	0.38	0.45	0.61	0.56	0.48	0.56	0.47	0.63
	MAE	TSS	1.85	1.8	1.52	1.53	1.30	1.34	1.38	1.42	1.36	1.27
	MAE	DMC	2.02	1.99	1.73	1.73	1.40	1.50	1.64	1.56	1.64	1.42
F	R2	TSS	0.28	0.36	0.56	0.57	0.73	0.73	0.68	0.66	0.69	0.71
	R2	DMC	0.31	0.36	0.52	0.54	0.73	0.7	0.62	0.65	0.63	0.7
	MAE	TSS	1.77	1.69	1.33	1.41	1.10	1.12	1.23	1.27	1.19	1.17
	MAE	DMC	1.88	1.87	1.54	1.60	1.19	1.25	1.41	1.37	1.41	1.28
SINGLE CULT.												
S	R2	TSS	0.48	0.42	0.41	0.46	0.54	0.5	0.46	0.44	0.46	0.53
	R2	DMC	0.43	0.38	0.3	0.41	0.5	0.46	0.29	0.42	0.2	0.47
	MAE	TSS	1.51	1.56	1.60	1.56	1.37	1.45	1.49	1.54	1.54	1.45
	MAE	DMC	1.70	1.75	1.88	1.77	1.57	1.63	1.83	1.70	1.92	1.66
F	R2	TSS	0.65	0.57	0.57	0.58	0.69	0.66	0.60	0.58	0.59	0.64
	R2	DMC	0.62	0.54	0.47	0.53	0.66	0.63	0.50	0.56	0.43	0.60
	MAE	TSS	1.27	1.38	1.36	1.41	1.18	1.23	1.31	1.35	1.33	1.28
	MAE	DMC	1.41	1.53	1.64	1.61	1.35	1.41	1.54	1.46	1.61	1.41

(multi-cultivar case) and once for a single overrepresented cultivar (single-cultivar case). Additionally, we evaluated the estimation success once for each individual spectral profile (single observations) and once for per-fruit average TSS and DMC estimates. The latter are computed by averaging both the reference and the estimated TSS and DMC values per single fruit (before computing statistics). The main findings are summarized in the following three subchapters.

3.1.1. Main results and comparison of regression models

On average, the best results were achieved by the RF algorithm, reaching a mean R^2 of 0.73 (MAE of 1.10° Brix and 1.19%) for per-fruit (F) averages, in the multi-cultivar case. The values are comparable for both TSS and DMC (97% correlated), with minor deviations due to uncorrelated errors in reference measurements (technique dependent, see Section 3.1.3). These results are similar to the state of the art achieved by other in-house developed prototypes, however with several advantages that will be discussed in detail in Section 4.1.

The estimates based on the single spectral profiles S are degraded relative to per-fruit averages F (- 0.12–0.16 R^2). As averaging can notably reduce estimation uncertainty, we presume a strong presence of random noise in measurements. This means that the estimates can be improved by further averaging spectral profiles. This will be feasible in the future use of the MSL technology, as multispectral point clouds can contain many redundant acquisitions per single fruit (see Section 3.4).

The ensemble of estimators (ESB.) marginally overperformed relative to RF (R^2 of 0.64 and 0.63 vs. 0.61) in the case of single spectral profiles (S), while other estimators underperformed. This indicates that further estimation improvements are possible by using a more complex regression model supported with a higher sample size.

The underperformance of PLS and LASSO regression relative to RF indicates that simple linear relationships between the reflectance values and the TSS and DMC are insufficient to model their association. Hence, without adequate prior data transformations and preprocessing, using PLSs is sub-optimal, despite being among the most established methods in the related literature.

Furthermore, using single variable predictors (x670 and IAD) showed limited success in modeling the distribution of TSS and DMC in the multi-cultivar case, requiring high generalizability of the regression model. Hence, the use of multispectral values brings significant benefits (R^2 of 0.73 vs. 0.28–0.36).

3.1.2. Single vs. multi-cultivar estimation

The most interesting observations are related to comparing the estimation success in the case of a model trained for all cultivars vs. a single cultivar. First, the results of RF are somewhat worse in the case of a single cultivar, which is unexpected. Namely, it is assumed that the variability of the observable fruit properties is smaller when constraining to a single cultivar, making training the estimation model easier. However, the RF successfully learned to generalize across different cultivars and it benefited from the increased sample size in the multi-cultivar case.

We made a brief investigation to confirm that the values reported in Table 3 for a multi-cultivar case are indeed representative of all

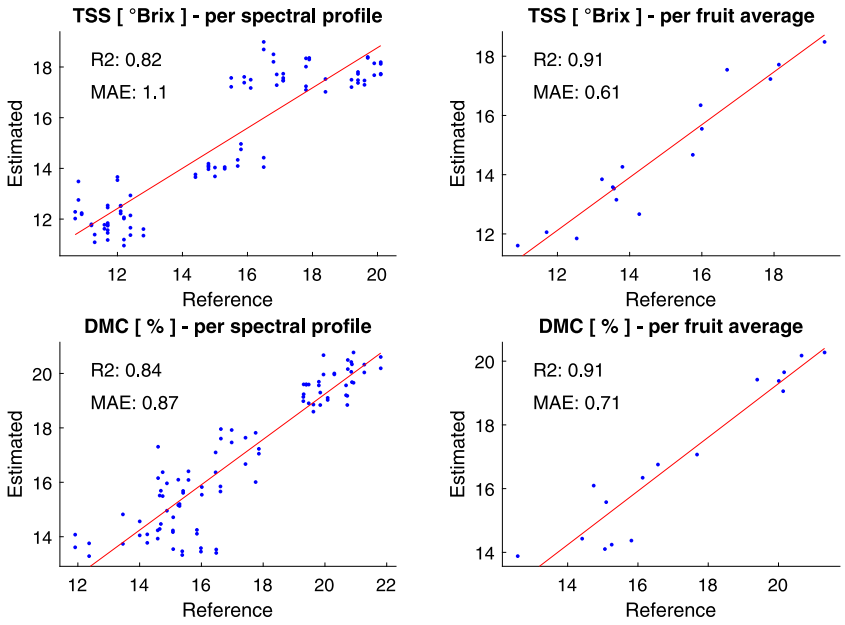

Fig. 4. The best case TSS and DMC estimation results (1 out of 100 runs) with the best performing algorithm (RF): estimate based on individual observations, i.e. spectral profiles (left); estimate based on per-fruit average of 6 observations (right).

cultivars in our dataset, as some of them are over and some underrepresented considering the sample size. For that, we used a bootstrapping-inspired approach where we computed per-cultivar MAEs based on all test data residuals and compared them. Although we observed some variability in the MAE values, the average MAE of eight cultivars (value not influenced by the sample size) was comparable to the values reported in Table 3 (approx. 10% lower). Hence, although, some variations in the estimation success can be expected for different apple cultivars, the data presented herein can be considered representative of all cultivars. The small mismatch in the reported MAEs can be partially attributed to the higher MAE of the overrepresented apple cultivar relative to others (see Table 1), which could explain the observable underperformance of the estimation model tuned for the single cultivar case.

A striking observation is that in the single-cultivar case, the single variable estimators only marginally underperform relative to RF. Hence, it seems that the main advantage of multispectral data is the possibility of generalization. The multispectral data is used for the internal classification of apples within the estimation algorithm, while it contributes less to the regression of the TSS and DMC values themselves.

This observation has a strong implication for the potential use cases. Namely, if the sufficient homogeneity of the fruits can be guaranteed, using a mono- or bichromatic LiDAR can be an effective way of remotely estimating TSS and DMC in apples. Additionally, using IAD vs. 670 nm alone showed no obvious benefits. Hence, our results suggest that a monochromatic LiDAR could be used as a substitute for handheld IAD devices allowing remote observations of certain fruit quality metrics. These observations will be further validated by a feature importance analysis in Section 3.2.

3.1.3. Best-case results and sample distribution

In Fig. 4 we present the best regression results using RF for a single most favorable test-train split out of 100 runs. This was done to increase the comparability of our results with similar studies that report statistics of a single run and have restricted sample size, e.g. Fan et al. (2020) and Mishra and Passos (2022). In this best-case scenario, the achieved R^2 of 0.91 and MAE of 0.61 °Brix for the per-fruit averaged TSS are already on the level sufficient for use in practice and are comparable to the state-of-the-art results achieved using handheld spectrometers (Section 4).

Visualizing the distribution of the individual estimates relative to reference values before and after averaging additionally highlights how effectively the results can be improved through per-fruit averaging, which is well achievable in the scanning setting as demonstrated in Section 3.4.

Finally, a noticeable difference in the distribution of corresponding data points for TSS and DMC shows that their estimates are not directly interchangeable despite high correlation. This indicates that the noise of the reference values is significantly contributing to overall variance in the data and that one of the limiting factors of the presented experiment is the lack of rigorous acquisition of the reference values in the dedicated laboratory, which could further positively impact the estimation results. However, we had no access to such facilities for our study.

3.2. Feature (wavelength) importance

The results of the feature importance analysis are summarized in Fig. 5. To achieve a more generalizable valuation, and, hence, a less dependent on the selected regression algorithm, we used five different mechanisms for feature importance estimation which are inherent to some of the implemented regression methods. More specifically, we estimated feature importance by: the absolute value of the weights of LASSO regression, variable importance in projection (VIP) scores in PLS, permuting out-of-bag observations (OOB), and summing gains in the mean squared error due to splits on each predictor (MSE) in RF, as well as MSE for the boosted decision trees. All 5 feature importance scores are normalized within the 0–1 range and stacked together.

The patterns observed in the figure support several hypotheses presented in the previous sections. First, the regression models for TSS and DMC are supported by the same wavelengths. Second, the whole width of the spectrum is used in the multi-cultivar case, while in the single-cultivar case, there is a clear peak centered around 670 nm related to the Chlorophyll A absorption. This explains the high estimation accuracy of a single-wavelength regression model in a single-cultivar case presented in Table 3, and confirms that multispectral data is of benefit for obtaining a more generalizable estimation.

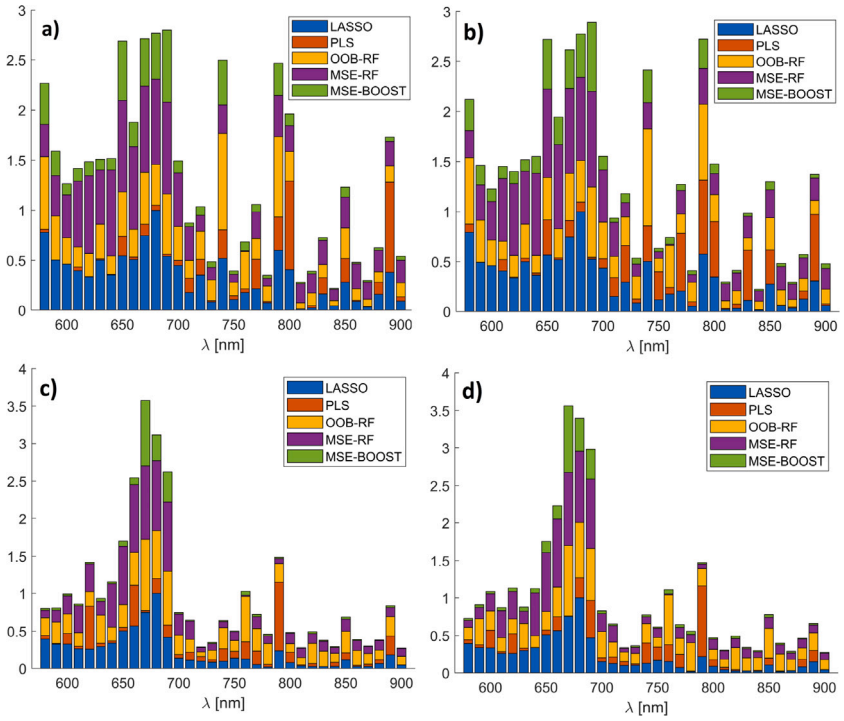

Fig. 5. Feature importance scores for all wavelengths calculated using 5 different mechanisms inherent to some of the used regression algorithms, normalized (0–1) and stacked together for generalizability: (a) TSS all cultivars, (b) DMC all cult., (c) TSS single cult., (d) DMC single cult.

In particular, the multivariate regression models use the whole observable region of the visible spectrum (580 nm – 750 nm) and only a few targeted wavelengths above 700 nm (740, 790, 800, 850, 890 nm). In Tran and Fukuzawa (2020), the authors reported that the following wavelengths were the highest contributors to the estimation of TSS (R^2 of 0.86): 680, 730, 760, 900 nm. Some overlap between the values exists, but it is not direct and further analysis needs to clarify if this is due to particular instrument properties, e.g., the favorable signal-to-noise ratio at particular wavelengths, due to fruit properties spawning through neighboring spectral channels, or both.

3.3. Range spectral profiles

Table 4 compares the results of TSS and DMC estimation in the following three cases: using reflectance spectra - RL (33 features), using reflectance and range spectra - RL + RG (66 features), and using range spectra alone - RG (33 features). The results are computed using the best performing algorithm (Random Forest) using all apple samples (All Cult.) and with the data processing as described in Section 2.4. The main observation is that range spectra do not improve the estimation results. On the contrary, likely due to the larger number of non-informative explanatory variables, the performance of the RF with 66 features is somewhat degraded (drop in R^2 of 1% for single spectra estimates and 6% for per-fruit mean estimates).

There are several possible hypotheses as to why the range spectra do not support the estimation. The first one is that the ranges do not carry information on TSS and DMC. However, this can be dismissed based on visual inspection of Fig. 3 (bottom) and observed correlations between range and reflectance spectra (Section 2.3). The second hypothesis is that range and reflectance carry the same information about TSS and DMC due to power-to-phase coupling, which was already suspected based on pre-analysis in Section 2.3. This hypothesis is supported by the estimation results based on range spectra alone (Table 4). The estimates are comparable to the RL ones, however, further degraded (drop in R^2 of 10%–15%). These observations are also reinforced by the feature importance analysis revealing that the same set of explanatory variables

Table 4
Estimating TSS [°Brix] and DMC [%] for all cultivars using RF by: reflectance (RL); reflectance and range (RL + RG); range spectra (RG); S – single spectra estimates; F – per-fruit mean estimates.

S/F	STATS.	VAR.	RL	RL + RG	RG
S	R2	TSS	0.61	0.61	0.55
	R2	DMC	0.61	0.60	0.52
	MAE	TSS	1.30	1.33	1.41
	MAE	DMC	1.40	1.47	1.61
F	R2	TSS	0.73	0.69	0.63
	R2	DMC	0.73	0.69	0.62
	MAE	TSS	1.10	1.19	1.27
	MAE	DMC	1.19	1.31	1.45

was used to make the predictions (visualization omitted as the plot is directly comparable to Fig. 5). Therefore, an additional investigation of this phenomenon will be necessary to eventually benefit from the spectrally resolved ranges in this use case. At this stage, they did not improve the regression results, although our previous work demonstrated that they can support the material classification (Han et al., 2022c).

There is a plausible reason why using range spectra was not advantageous in this work, although it was helpful in material classification. Namely, the laser beam of our prototype falls at somewhat different locations on the sampled surface depending on the wavelength. The positional changes of the footprint location are approx. of the same size as the footprint diameter (6–8 mm). For reflectance data, this poses no issues as apple properties change gradually (inhomogeneity becomes apparent only over larger distances). However, as apples have varying surface curvatures, the measured ranges do not depend only on the material properties, but also on the local surface curvature. Hence, the information related to TSS and DMC could be superimposed by the information about the apple's shape. This limitation of the current prototype needs to be overcome to take advantage of spectrally resolved range measurements when measuring non-planar surfaces.

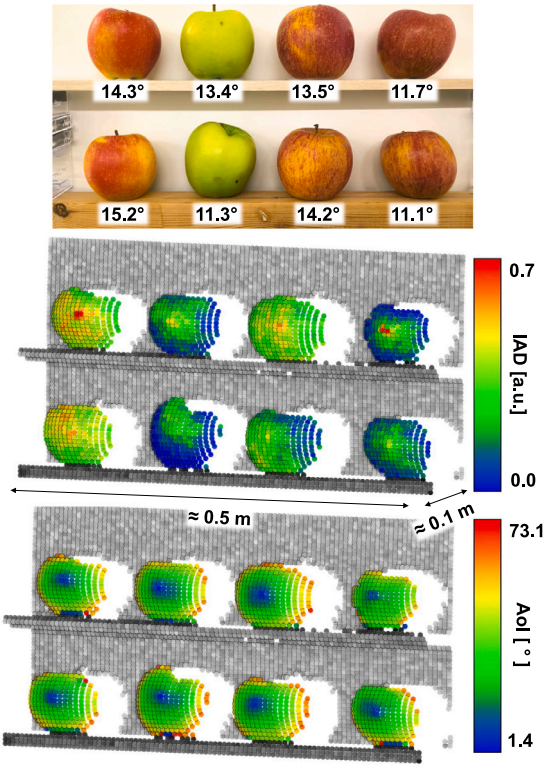

Fig. 6. Apples scanned with our multispectral LiDAR prototype at ≈ 5 m stand-off range; RGB image with average TSS value in °Brix provided for each fruit (top); corresponding 3D point clouds colored by per-point IAD values (middle) and AoI values (bottom).

3.4. Demo of scanning capabilities

We additionally conducted a demonstration of how the results presented in Section 3.1 relate to a prospective use case of multispectral laser scanning of fruits at larger distances. The spectral profiles were collected using the setup with a scanning unit (Fig. 1, right) and a spectrometer (Section 2.2), while reference measurements were acquired along the whole scanned surface of eight apples (6 samples per fruit; procedure as described in 2.1).

Fig. 6 presents an RGB image and point clouds of eight apples scanned at a 5 m distance. We semi-arbitrarily chose two fruit samples of four cultivars, governed by the fruit availability in the local supermarket and by a desire to achieve noticeable variability in TSS and DMC values. The samples of different cultivars were distributed in two corresponding rows with the following distribution from left to right: 2x Kanzi, 2x Greenstar, 2x Kiku, 2x Braubern (Fig. 6 (top)).

Fig. 6 (middle) presents the point cloud colored by the IAD index values calculated from the per-point obtained spectral profiles. We used IAD instead of TSS or DMC predictions based on the models from Section 3.1 as the spectral profiles collected with this setup were discretized by 1914 channels of 0.17 nm bandwidth (see Section 2.2). Hence, this data and the trained regression models are not compatible. Also, we did not use the reflectance at 670 nm alone due to instrument-related systematic effects, which were partially canceled out by introducing a spectral index, as they had a similar impact across all wavelengths.

The IAD index was successful in approximating TSS and DMC based on the multispectral 3D point cloud data. The IAD indices in Fig. 6 (middle) show a clear distinction between the fruits with different TSS and DMC, which corresponds to the destructive reference measurements given in Fig. 6 (top). We used per-single-point (S) and per-fruit averaged (F) IAD values to estimate TSS and DMC using simple linear regression. Fig. 7 presents the results for TSS (DMC directly comparable).

The per-fruit averaged IAD values (F) can successfully approximate TSS with R^2 of 0.74, which is directly comparable to the results presented in Section 3.1.1. The statistics based on 8 data points (Fig. 7, blue diamonds) has limited power, however, both LiDAR and reference values were generated by averaging many observations (3 readings at 6 locations per fruit for reference values and averaging all single points per fruit; Fig. 7, orange points). Hence, although the exact statistical quantities cannot be well generalized, they indicate that the results presented in Section 3.1 can be extended to measurements at higher distances with simultaneous acquisition of geometrical data (i.e. acquisition of point clouds).

With this setup, we achieved good initial results in modeling relative TSS and DMC content across four different apple cultivars using a single variable predictor, the IAD index. This is contradictory to the observations presented in Table 3, where IAD performs well only in the single-cultivar case. Moreover, the achieved MAE of 0.58° Brix is 47% smaller than the best one achieved in Section 3.1.1. If this is due to averaging a higher number of spectral and reference observations, changes in our experimental setup (e.g. higher sensitivity of narrower spectral bands) or related to the properties of the four sub-selected apple cultivars should be further investigated.

The per-single-point (S) IAD values are notably more scattered (Fig. 7, orange points) than per fruit averages (F), resulting in the R^2 of only 0.44. We argue that the reason for this is partially the noise of the individual point estimates (corroborated by the drop in MAE of 32% through point averaging) and partially the systematic effects superimposing our IAD values, primarily, the angle of incidence (AoI) effect. The AoI is known to significantly impact the spectral measurements of plant materials regardless of the used measurement technology (Behmann et al., 2016) and it cannot be canceled by generating simple ratios between the spectral channels (e.g. by IAD index), as the effect depends on the wavelength.

The simultaneous acquisition of geometrical and spectral data in the form of the 3D multispectral point clouds (Fig. 6) allows for calculating the angle of incidence between the light beams and the fruit surface, enabling the possibility of investigating the relationship between AoI and spectral data.

Fig. 6 (middle) vs. (bottom) shows that the distribution of IAD values roughly follows the distribution of AoIs. This observation is corroborated by the significant negative correlations (Spearman's rank correlation coefficient, > 99% probability) between AoIs and IAD values for each of the eight fruits, reaching values of −68% (−48% in average). This points out that increasing the quality of per-single-point (S) TSS estimation and mapping local variations of fruit properties will require further research related to the radiometric calibration of backscattered light. Such efforts are out of the scope of this work. However, the technology presented herein provides the tools for facilitating this research, as the simultaneous acquisition of geometry and spectrum allow for establishing functional relationships between the variables and eventually establishing the data-driven radiometric correction approaches.

4. Discussion

We demonstrated that TSS and DMC can be estimated remotely from spectral profiles acquired by a multispectral LiDAR instrument, achieving minimum uncertainty (MAE) of 1.10 °Brix for TSS and 1.19% for DMC, and R^2 value of 0.73 for both fruit quality parameters. These results fall somewhat short of the recent results achieved with commercial handheld spectrometers (Table 5). However, they are achieved with the fruit samples measured at 0.5 m stand-off distance under uncontrolled illumination, hence, not requiring direct contact with the fruit nor dark chambers to facilitate successful measurements.

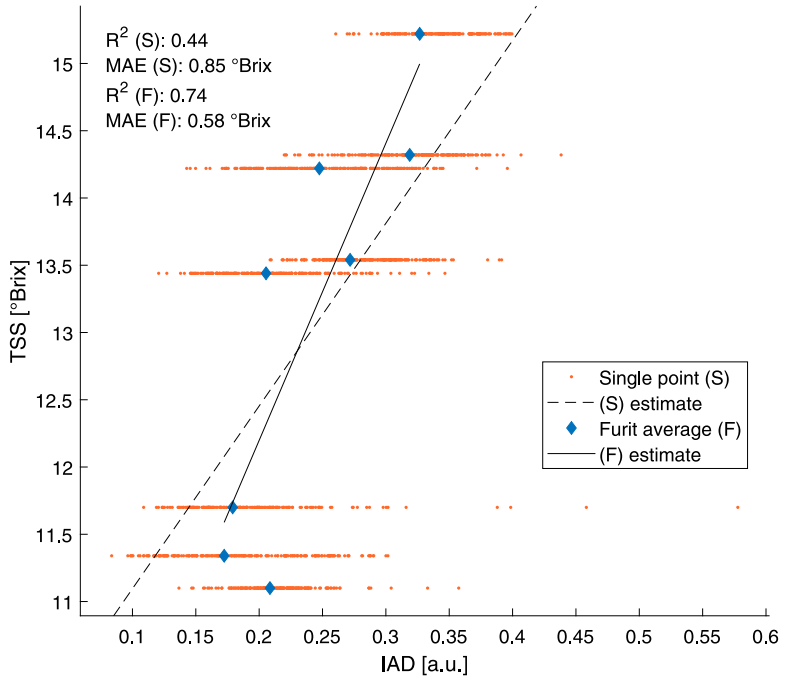

Fig. 7. Estimation of TSS by IAD values (extracted from multispectral 3D point clouds) using simple linear regression: S – based on individual spectral profiles (single data points), F – based on per-fruit averages.

Table 5
Summary of the reported fruit TSS and DMC estimation successes using portable spectrometers working in VIS/NIR range (Cultivars: S – single cult., M – multiple cult., Instrument "I.": C – commercial, P - prototype).

Value	Amount	CULT.	Data	Data processing	I.	REF.
R^2_{TSS}	0.81	S	17004 samples, 1 orchard, 3 seasons	PLS, no preprocessing	C	Biegert et al. (2021)
R^2_{DMC}	0.91	M	2252 samples, 1 orchard, 1 season, rigorous reference measurements	extensive preprocessing, PLS	C	Mishra and Passos (2021)
R^2_{DMC}	0.83, 0.89	M	2252 samples, 2 seasons	PLS, preprocessing	C	Teh et al. (2020)
R^2_{TSS}	0.95[b], 0.85[c]	S	625 samples	PLS, extensive vs no preprocessing	C	Mishra et al. (2021a)
R^2_{TSS}; R^2_{DMC}	0.55–0.81[a]; 0.83–0.88[a]	M	1400 samples, 1 orchard, multiple seasons	PLS, preprocessing, differing training/validation splits	C	Kumar et al. (2015)
R^2_{TSS}; R^2_{DMC}	0.90; 0.92	M	1575 samples, multiple orchards, multiple seasons	PLS	C	Zhang et al. (2019)
R^2_{TSS}; R^2_{DMC}	0.88; 0.81	S	551 samples, 1 local vendor	1D-CNNs, best run report	C	Mishra (2022)
R^2_{TSS}	0.77	S	440 samples, 3 vendors	PLS, preprocessing, 1 run report with random data split	P	Fan et al. (2020)
R^2_{TSS}	0.86	S	80 × 2 samples, 1 supermarket	PLS, preprocessing	P	Tran and Fukuzawa (2020)
R^2_{TSS}; R^2_{DMC}	0.73; 0.73	M	80 × 6 samples, 1 supermarket	Random-forest, no preprocessing	P	**Ours**

[a] R^2 values of different training and validation splits (estimated based on the reported correlation coefficients).
[b] Extensive preprocessing.
[c] No preprocessing.

To summarize information from Table 5, combining established hardware and software regularly achieves the performance of around 0.85–0.90 R^2 for both values of interest, while the maximum performance with sophisticated regression models and extensive preprocessing reaches 0.95 R^2. However, the studies analyzing the performance of self-developed prototypes report a success of 0.75–0.85 R^2, which is comparable to our results. Since we deploy a novel sensing technique, which brings all the technical challenges of early development, a further increase in estimation accuracy can be expected (see Section 4.1). In contrast, the spectrometers paired with active illumination by broadband incoherent light sources (e.g. LED lights) and requiring direct contact with the fruit are present and continuously developing within this domain for more than three decades (Watada, 1993).

Furthermore, in Section 3.4 we demonstrated TSS and DMC estimation at even larger stand-off distances ($\approx$ 5 m), which could technologically be further expanded to tenths or hundreds of meters. This could allow sensing at distances that are out of reach of competing technologies, such as hyperspectral cameras, and would, therefore, allow for new use cases, primarily related to outdoor on-tree estimation over whole fruit orchards.

Finally, we demonstrated the possibility of simultaneous acquisition of geometrical (3D point clouds) and spectral data. The latter capability

opens possibilities of simultaneously monitoring inner (e.g. demonstrated TSS and DMC) and outer (shape and size) fruit quality factors, which are of relevance for a number of applications as well (Musacchi and Serra, 2018). An additional important aspect of acquiring geometrical data along with spectral is facilitating the radiometric correction due to the angle of incidence effect. The effect is known to systematically impact the acquired spectral data (see e.g. results in Section 3.4), irrespective of the used sensor type, and is recognized as a significant hindrance in plant phenotyping (Behmann et al., 2016). Facilitating such a radiometric correction for hyperspectral imagery is not trivial, as it would require the deployment of additional sensors for 3D geometry acquisition and elaborate data integration workflows. Hence, this highlights the additional relevant advantage of the MSL relative to the established imaging technologies.

In the discussion above, we have highlighted the main advantages of using the demonstrated sensing technology relative to the state-of-the-art solutions. In the following sub-chapters, we discuss the limitations of our study, the possibilities for future improvements, and the aspects related to the generalizability and transferability of our findings to prospective use cases.

4.1. Study limitations and future improvements

Multiple limitations of our study are potentially impacting the estimation success in the conducted experiment, such as: limited sample size for training regression models; lack of sophisticated preprocessing; limited accuracy of reference measurements; limited precision of individual spectral profiles; acquired spectral data either missing some information for estimation or being superimposed by other systematic effects (e.g. disproportionally strong direct reflection from the fruit surface relative to the beams penetrating to fruit tissue, angle of incidence effect); sub-optimal experiment design choices (e.g. inconsistency of 2 cm thick apple samples for destructive measurements relative to the expected light penetration depth, or using too wide bandwidths of individual spectral channels).

However, there are many possibilities for addressing these challenges, besides conducting a more rigorous experiment. First, simply acquiring a higher sample size would allow for training more complex regression models, where deep learning algorithms, such as CNNs, were proven to achieve state-of-the-art performance (Mishra and Passos, 2021). Additionally, algorithms such as 3D CNNs and PointNet could be directly applied to multispectral point clouds of individual fruits and eventually extract further information from the spatial variations in the reflectance values. Alternatively, averaging more spectral profiles per fruit, feature engineering, and intelligent preprocessing, e.g. by utilizing the PORTO method, can enhance the signal and dampen the noise impact of irrelevant spectral features (Mishra et al., 2021b). Finally, signal-to-noise ratio and sensitivity could be enhanced by further manipulation of LiDAR components and settings, e.g. by exchanging our components with incoherent supercontinuum lasers or new generation supercontinuum frequency comb lasers, adjusting power distribution over spectral profiles, increasing integration time, optimizing beam properties (focal point, beam waist, and divergence angle), etc.

Furthermore, the LiDAR data could be supplemented by additional information provided by inexpensive sensors such as RGB cameras. We presume that this could help to separate superimposed signals at the most critical wavelengths centered around 670 nm, particularly the superimposed signals of visible fruit color and absorption of chlorophyll A in fruit mesocarp.

Also, additional information can be obtained already by further exploiting the observations of the herein-presented active remote sensing technique. As demonstrated, the prototype we used provides spectrally resolved range measurements which are proven to carry additional information about material properties relative to the reflectance data (Han et al., 2022c). Although that information source did not support the estimation results in this work, it is possible that this could be changed if the technical limitations of the setup are resolved (Section 3.3).

Besides range spectra, there is a possibility of using a rotating linear polarizer in the MSL prototype (Han et al., 2022a) to separate the polarized and unpolarized components of the backscattered light from objects, which could decouple the signal directly reflected from the surface of the fruit and the part of the signal de-polarized by scattering from inner fruit tissue. This could help resolve the mentioned problems of super-imposed signals, as well as increase the sensitivity to the components of the signal that are of primary interest. Moreover, this technology allows for tracking the angle and degree of linear polarization as additional signal features, which were proven to be useful for enhanced material probing (Han et al., 2023) and could support fruit quality estimation as well.

4.2. Generalizability and transferability of the results

An important aspect of our results requiring attention is that using multiple spectral channels instead of one primarily helps with regression model generalizability. This is relevant, as ideally, the TSS and DMC estimation should be applicable across fruit cultivars, maturity stages, and orchards with different soil and atmospheric properties, as well as across growing seasons, without extensive recalibration of the estimation models.

Nevertheless, relative TSS and DMC within a specific homogenous subspace seem to be to a large degree explained by a single wavelength. This is important information for the practitioners, as monochromatic LiDAR is readily available, it is cheaper, and it could be already implemented, as it was demonstrated in the case of monitoring banana ripening (Saha and Zude-Sasse, 2022). This approach would, however, require repeated model calibrations for specific datasets.

Another aspect relevant to the transferability of our results to real application cases is the likely necessity for calibrating the TSS and DMC estimates for the impact of temperature. Based on the experiences with comparable reflectance spectroscopy devices, such calibration could be simply facilitated by incorporating additional observations of the ambient temperature into the regression model (Peirs et al., 2003). However, investigating this is out of the scope of our work, as our prototype is currently not portable and we cannot notably manipulate the ambient temperature in our laboratory.

Finally, in our work, we focused on a subset of fruit quality metrics that had strong evidence supporting their estimation using VIS-NIR reflectance spectroscopy. Current research suggests that commercial handheld spectrometers are either less sensitive or not fit for estimating further relevant fruit metrics such as titratable acidity, fruit firmness, and starch (Wang et al., 2015).

Active sensing with LiDAR can potentially offer more opportunities than handheld spectrometers by exploiting the information beyond reflectance. Firstly, spectrally resolved ranges, which among others carry the information about laser beam penetration depth, could be related to the material properties such as material density (Han et al., 2022b), which could be linked to the fruit firmness. Secondly, we plan to investigate if tracking the changes in the polarization of the emitted laser beam could hold some proxies for further quantities of interest. However, the sizeable benefits of the latter exploration will likely require substantial further instrumental development and research efforts due to the high complexity of the interaction of polarized light with biological tissues (Ghosh, 2013).

5. Conclusion

Within this work, we demonstrated that multispectral LiDAR, working in the VIS-NIR spectral range, can be used to remotely sense certain fruit quality metrics. This bypasses the requirement of (near-)direct contact with the fruit or controlled illumination conditions (dark

chambers), which are prerequisites of standard methods used in chemometrics. We demonstrated this in a case study of estimating total soluble solids (TSS) and dry matter content (DMC) of store-bought apples of different cultivars at a distance of approximately 0.5 m. Random forest regression models topped the performance of commonly used partial least squares (PLS) and achieved 0.73 R^2 for estimating both values of interest, with a mean absolute error of 1.10 °Brix for TSS and 1.19% for DMC. Further analysis revealed that the main contribution in the estimation can be credited to chlorophyll A absorption peak at 670 nm, which is a key component of the IAD index used to track fruit maturity. Moreover, in the case when the regression was done only on a single cultivar, the reflectance at 670 nm alone had a comparable performance relative to the random forest estimates. This indicates that the primary role of further spectral channels is in assuring a more generalizable regression model. Finally, in a small-scale additional experiment, we generated multispectral 3D point clouds of several apples at a 5 m distance. We demonstrated that the abovementioned observations are transferable to sensing at larger distances and to multispectral scanning, which allows for the simultaneous acquisition of spectral and geometrical data on analyzed fruits with a single system.

Our work presents a first attempt at using a mode-locked femtosecond supercontinuum-based multispectral LiDAR in this application domain. Hence, the study has its limitations, primarily a relatively small sample size compared to similar investigations in the literature. In future work, we aim to generate a more robust and generalizable evaluation of the methodology potential for estimating fruit quality metrics by expanding the number and diversity of measurement subjects. Furthermore, we plan to explore the possibility of enhancing the results and estimating further relevant fruit quality parameters by supplementing the input data with phase delay spectral profiles, by exploring the benefits of tracking the laser light polarization, and by integrating further measurements of inexpensive additional sensors such as RGB cameras.

CRediT authorship contribution statement

Tomislav Medic: Conceptualization, Formal analysis, Funding acquisition, Investigation, Project administration, Software, Validation, Visualization, Writing – original draft. **Pabitro Ray:** Methodology, Writing – original draft. **Yu Han:** Methodology, Writing – original draft. **Giovanni Antonio Lodovico Broggini:** Conceptualization, Writing – review & editing. **Simon Kollaart:** Conceptualization, Writing – review & editing.

Declaration of competing interest

The authors declare that they have no known competing financial interests or personal relationships that could have appeared to influence the work reported in this paper.

Data availability

Data will be made available on request.

Acknowledgments

This work was supported by an ETH Zurich Postdoctoral Fellowship, Switzerland.

References

Abasi, S., Minaei, S., Jamshidi, B., Fathi, D., 2018. Dedicated non-destructive devices for food quality measurement: A review. Trends Food Sci. Technol. 78, 197–205.
Azodanlou, R., 2001. A Methodology for Assessing the Quality of Fruit and Vegetables. ETH Zurich.
Behmann, J., Mahlein, A.-K., Paulus, S., Dupuis, J., Kuhlmann, H., Oerke, E.-C., Plümer, L., 2016. Generation and application of hyperspectral 3D plant models: methods and challenges. Mach. Vis. Appl. 27, 611–624.
Biegert, K., Stöckeler, D., McCormick, R.J., Braun, P., 2021. Modelling soluble solids content accumulation in 'braeburn' apples. Plants 10 (2), 1–16.
Chen, Y., Räikkönen, E., Kaasalainen, S., Suomalainen, J., Hakala, T., Hyyppä, J., Chen, R., 2010. Two-channel hyperspectral LiDAR with a supercontinuum laser source. Sensors 10 (7), 7057–7066.
Du, L., Gong, W., Shi, S., Yang, J., Sun, J., Zhu, B., Song, S., 2016. Estimation of rice leaf nitrogen contents based on hyperspectral LIDAR. Int. J. Appl. Earth Obs. Geoinf. 44, 136–143.
Eitel, J., Höfle, B., Vierling, L., Abellán, A., Asner, G., Deems, J., Glennie, C., Joerg, P., LeWinter, A., Magney, T., Mandlburger, G., Morton, D., Müller, J., Vierling, K., 2016a. Beyond 3-D: The new spectrum of lidar applications for earth and ecological sciences. Remote Sens. Environ. 186, 372–392.
Eitel, J., Vierling, L., Long, D., 2010. Simultaneous measurements of plant structure and chlorophyll content in broadleaf saplings with a terrestrial laser scanner. Remote Sens. Environ. 114 (10), 2229–2237.
Eitel, J., Vierling, L., Long, D., Hunt, E., 2016b. Early season remote sensing of wheat nitrogen status using a green scanning laser. Agricult. Forest Meteorol. 151 (10), 1338–1345.
Elsherif, A., Gaulton, R., Mills, J., 2018. Estimation of vegetation water content at leaf and canopy level using dual-wavelength commercial terrestrial laser scanners. Interface Focus 8 (2), 372–392.
Fan, S., Wang, Q., Tian, X., Yang, G., Xia, Y., Li, J., Huang, W., 2020. Non-destructive evaluation of soluble solids content of apples using a developed portable vis/NIR device. Biosyst. Eng. 193, 138–148.
Gaulton, R., Danson, F., Ramirez, F., Gunawan, O., 2013. The potential of dual-wavelength laser scanning for estimating vegetation moisture content. Remote Sens. Environ. 132, 32–39.
Ghosh, N., 2013. Tissue polarimetry: concepts, challenges, applications, and outlook. J. Biomed. Opt. 16 (11), 110801.
Goisser, S., Wittmann, S., Mempel, H., 2021. Food-scanner applications in the fruit and vegetable sector. Landtechnik 76 (1), 52–67.
Grinsztajn, L., Oyallon, E., Varoquaux, G., 2022. Why do tree-based models still outperform deep learning on typical tabular data? In: 36th Conference on Neural Information Processing Systems (NeurIPS 2022) Track on Datasets and Benchmarks.
Hakala, T., Nevalainen, O., Kaasalainen, S., Mäkipää, R., 2015. Technical note: Multispectral lidar time series of pine canopy chlorophyll content. Biogeosciences 12 (5), 1629–1634.
Hakala, T., Suomalainen, J., Kaasalainen, S., Chen, Y., 2012. Full waveform hyperspectral LiDAR for terrestrial laser scanning. Opt. Express 20 (7), 7119–7127.
Han, Y., Salido-Monzú, D., Butt, J., Wieser, A., 2022a. Polarimetric femtosecond-laser LiDAR for multispectral material probing. In: SPIE Proc. Optics and Photonics for Advanced Dimensional Metrology I. Vol. 12137, 1213708.
Han, Y., Salido-Monzú, D., Wieser, A., 2022b. Comb-based multispectral LiDAR providing reflectance and distance spectra. Opt. Express 30 (23), 42362–42375.
Han, Y., Salido-Monzú, D., Wieser, A., 2022c. Delay-augmented spectrometry for target classification using a frequency-comb LiDAR. In: CLEO: Science and Innovations. Optica Publishing Group, pp. SF2F–5.
Han, Y., Salido-Monzú, D., Wieser, A., 2023. Classification of material and surface roughness using polarimetric multispectral LiDAR. Opt. Eng. 62 (11), 114104–114104.
Jiao, Y., Li, Z., Chen, X., Fei, S., 2020. Preprocessing methods for near-infrared spectrum calibration. J. Chemom. 34 (11).
Jin, S., Sun, X., Wu, F., Su, Y., Li, Y., Song, S., Xu, K., Ma, Q., Baret, F., Jiang, D., Ding, Y., Guo, Q., 2021. Lidar sheds new light on plant phenomics for plant breeding and management: Recent advances and future prospects. ISPRS J. Photogramm. Remote Sens. 171, 202–223.
Junttila, S., Hölttä, T., Katoh, M., Vastaranta, M., Kaartinen, H., Holopainen, M., Hyyppä, H., 2021. Lidar sheds new light on plant phenomics for plant breeding and management: Recent advances and future prospects. ISPRS J. Photogramm. Remote Sens. 255 (112274).
Junttila, S., Kaasalainen, S., Vastaranta, M., Hakala, T., Nevalainen, O., Holopainen, M., 2015. Nvestigating bi-temporal hyperspectral lidar measurements from declined trees-experiences from laboratory test. Remote Sens. 7 (10), 13863–13877.
Kaasalainen, S., Åkerblom, M., Nevalainen, O., Hakala, T., Kaasalainen, M., 2018. Uncertainty in multispectral lidar signals caused by incidence angle effects. Interface Focus 8 (2).
Kaasalainen, S., Nevalainen, O., Hakala, T., Anttila, K., 2016. Incidence angle dependency of leaf vegetation indices from hyperspectral lidar measurements. Photogramm. Fernerkund. Geoinf. 2016 (2), 75–84.
Kumar, S., McGlone, A., Whitworth, C., Volz, R., 2015. Postharvest performance of apple phenotypes predicted by near-infrared (NIR) spectral analysis. Postharvest Biol. Technol. 100, 16–22.

LeCun, Y., Bottou, L., Orr, G., Müller, K., 2012. Efficient BackpProp. In: Neural Networks: Tricks of the Trade.
Li, W., Sun, G., Niu, Z., Gao, S., Qiao, H., 2014. Estimation of leaf biochemical content using a novel hyperspectral full-waveform LiDAR system. Remote Sens. Lett. 5 (8), 693–702.
Magney, T., Eusden, S., Eitel, J., Logan, B., Jiang, J., Vierling, L., 2014. Assessing leaf photoprotective mechanisms using terrestrial LiDAR: Towards mapping canopy photosynthetic performance in three dimensions. New Phytol. 201 (1), 344–356.
Mahanti, N., Pandiselvam, R., Kothakota, A., Ishwarya, S., Chakraborty, S., Kumar, M., Cozzolino, D., 2022. Emerging non-destructive imaging techniques for fruit damage detection: Image processing and analysis. Trends Food Sci. Technol. 120, 418–438.
Malkamäki, T., Kaasalainen, S., Ilinca, J., 2019. Portable hyperspectral lidar utilizing 5 GHz multichannel full waveform digitization. Opt. Express 27 (8), A468.
Mcglone, V., Jordan, R., Seelye, R., Clark, C., 2003. Dry-matter - a better predictor of the post-storage soluble solids in apples? Postharvest Biol. Technol. 28, 431–435.
Minoshima, K., Matsumoto, H., 2000. High-accuracy measurement of 240-m distance in an optical tunnel by use of a compact femtosecond laser. Appl. Opt. 39 (30), 5512–5517.
Mishra, P., 2022. Bypassing NIR pre-processing optimization with multiblock pre-processing ensemble approaches. NIR News 33 (7–8), 5–8.
Mishra, P., Passos, D., 2021. A synergistic use of chemometrics and deep learning improved the predictive performance of near-infrared spectroscopy models for dry matter prediction in mango fruit. Chemometr. Intell. Lab. Syst. 212 (104287).
Mishra, P., Passos, D., 2022. Multi-output 1-dimensional convolutional neural networks for simultaneous prediction of different traits of fruit based on near-infrared spectroscopy. Postharvest Biol. Technol. 183.
Mishra, P., Roger, J., Marini, F., Biancolillo, A., Rutledge, D., 2021a. FRUITNIR-GUI: A graphical user interface for correcting external influences in multi-batch near infrared experiments related to fruit quality prediction. Postharvest Biol. Technol. 175.
Mishra, P., Roger, J., Marini, F., Biancolillo, A., Rutledge, D., 2021b. Parallel pre-processing through orthogonalization (PORTO) and its application to near-infrared spectroscopy. Chemometr. Intell. Lab. Syst. 212.
Mishra, P., Verschoor, J., Nijenhuis-de Vries, M., Polder, G., Boer, M.P., 2023. Portable near-infrared spectral imaging combining deep learning and chemometrics for dry matter and soluble solids prediction in intact kiwifruit. Infrared Phys. Technol. 131, 104677.
Musacchi, S., Serra, S., 2018. Apple fruit quality: Overview on pre-harvest factors. Sci. Hort. 234, 409–430.
Nevalainen, O., Hakala, T., Suomalainen, J., Mäkipää, R., Peltoniemi, M., Krooks, A., Kaasalainen, S., 2014. Fast and nondestructive method for leaf level chlorophyll estimation using hyperspectral LiDAR. Agricult. Forest Meteorol. 198, 250–258.
Niu, Z., Xu, Z., Sun, G., Huang, W., Wang, L., Feng, M., Li, W., He, W., Gao, S., 2015. Design of a new multispectral waveform LiDAR instrument to monitor vegetation. IEEE Geosci. Remote Sens. Lett. 12 (7), 1506–1510.
Pathmanaban, P., Gnanavel, B., Anandan, S., 2019. Recent application of imaging techniques for fruit quality assessment. Food Sci. Technol. 94, 32–42.
Peirs, A., Scheerlinck, N., Nicolai, B.M., 2003. Temperature compensation for near infrared reflectance measurement of apple fruit soluble solids contents. Postharvest Biol. Technol. 30 (3), 233–248.
Peirs, A., Scheerlinck, N., Nicolai, B., 2019. Temperature compensation for near-infrared reflectance measurement of apple fruit soluble solids content. Postharvest Biol. Technol. 30 (3), 233–248.
Pu, R., 2017. Hyperspectral Remote Sensing: Fundamental and Principles. CRC Press.
Puttonen, E., Soumalainen, J., Hakala, T., Räikkönen, E., Kaartinen, H., Kaasalainen, S., Litkey, P., 2010. Trees species classification from fused active hyperspectral reflectance and LIDAR measurements. Forest Ecol. Manag. 260 (10), 1846–1852.
Ray, P., Salido-Monzú, D., Camenzind, S.L., Wieser, A., 2023. Supercontinuum-based hyperspectral LiDAR for precision laser scanning. Opt. Express 31 (20), 33486–33499.
Saha, K., Zude-Sasse, M., 2022. Estimation of chlorophyll content in banana during shelf life using LiDAR laser scanner. Postharvest Biol. Technol. 192.
Salido-Monzú, D., Wieser, A., 2018. Simultaneous distance measurement at multiple wavelengths using the intermode beats from a femtosecond laser coherent supercontinuum. Opt. Eng. 57 (4), 044107.
Snoek, J., Larochelle, H., Adams, R., 2012. Practical bayesian optimization of machine learning algorithms. ArXiv.
Srivastava, S., Sadistap, S., 2018. Non-destructive sensing methods for quality assessment of on-tree fruits: a review. J. Food Meas. Charact. 12 (1), 497–526.
Sun, J., Shi, S., Gong, W., Yang, J., Du, L., Song, S., Chen, B., Zhang, Z., 2017. Evaluation of hyperspectral LiDAR for monitoring rice leaf nitrogen by comparison with multispectral LiDAR and passive spectrometer. Sci. Rep. 7.
Teh, S., Coggins, J., Kostick, S., Evans, K., 2020. Location, year, and tree age impact NIR-based postharvest prediction of dry matter concentration for 58 apple accessions. Postharvest Biol. Technol. 166.
Tran, N., Fukuzawa, M., 2020. A portable spectrometric system for quantitative prediction of the soluble solids content of apples with a pre-calibrated multispectral sensor chipset. Sensors 20 (20), 1–11.
Vosselman, G., Maas, H., 2010. Airborne and Terrestrial Laser Scanning. CRC Press.
Wang, H., Peng, J., Xie, C., Bao, Y., He, Y., 2015. Fruit quality evaluation using spectroscopy technology: A review. Sensors 15 (5), 11889–11927.
Watada, A., 1993. Methods for determining quality of fruits and vegetables. In: International Symposium on Quality of Fruit and Vegetables: Influence of Pre-and Post-Harvest Factors and Technology. Vol. 379, pp. 559–568.
Wold, S., Sjostrom, M., Eriksson, L., Sweden, S., 2001. PLS-regression: a basic tool of chemometrics. Chemometr. Intell. Lab. Syst. 58, 109–130.
Zhang, Y., Nock, J., Shoffe, Y., Watkins, C., 2019. Non-destructive prediction of soluble solids and dry matter contents in eight apple cultivars using near-infrared spectroscopy. Postharvest Biol. Technol. 151, 111–118.
Zhu, X., Wang, T., Darvishzadeh, R., Skidmore, A., Niemann, K., 2015. 3D leaf water content mapping using terrestrial laser scanner backscatter intensity with radiometric correction. ISPRS J. Photogramm. Remote Sens. 110, 14–23.